Temperature- and doping-dependent nanoscale Schottky barrier height at the Au/Nb:SrTiO$_3$ interface

R. Buzio, A. Gerbi, E. Bellingeri, and D. Marré

Temperature- and doping-dependent nanoscale Schottky barrier height at the Au/Nb:SrTiO$_3$ interface

R. Buzio,[1,a)] A. Gerbi,[1] E. Bellingeri,[1] and D. Marré[1,2]

[1]*CNR-SPIN, C.so F.M. Perrone 24, 16152 Genova, Italy*
[2]*Physics Department, University of Genova, Via Dodecaneso 33, 16146 Genova, Italy*

We use ballistic electron emission microscopy to investigate prototypical Au/Nb-doped SrTiO$_3$ (NSTO) Schottky barrier diodes for different temperatures and doping levels. To this end, ultrathin Au overlayers are thermally evaporated onto TiO$_2$-terminated NSTO single crystal substrates. We show that at room temperature, regardless of the nominal doping, rectification is controlled by a spatially inhomogeneous Schottky barrier height (SBH), which varies on a length scale of tens of nanometers according to a Gaussian distribution with a mean value of 1.29–1.34 eV and the standard deviation in the range of 80–100 meV. At lower temperatures, however, doping effects become relevant. In particular, junctions with a low Nb content of 0.01 and 0.05 wt. % show an ~300 meV decrease in the mean SBH from room temperature to 80 K, which can be explained by an electrostatic analysis assuming a temperature-dependent dielectric permittivity for NSTO. In contrast, this model fails to predict the weaker temperature dependence of SBH for junctions based on 0.5 wt. % NSTO. Our nanoscale investigation demands to reassess conventional models for the NSTO polarizability in high-intensity electric fields. Furthermore, it contributes to the comprehension and prediction of transport in metal/SrTiO$_3$ junctions and devices. *Published by AIP Publishing.* https://doi.org/10.1063/1.5049635

The interface between large work function metals (e.g., Au, Pt, Ag…) and *n*-type Nb-doped SrTiO$_3$ (NSTO) single crystals attracts great attention for its rich and yet not well-understood phenomenology.[1–12] In fact, the response of such Schottky contacts turns out to be extremely sensitive to the processing conditions so that largely different transport properties have been reported so far, even for the same nominal system. Specifically, a variety of behaviours spanning from high-quality rectification to hysteretic bipolar resistive switching (RS) are found from room temperature (RT) to ~200 K,[1,13] whereas a peculiar polarity reversal progressively dominates the junction response at an even lower temperature.[7,14] Importantly, an unintentional low-permittivity "dead layer" is often claimed to be formed in the NSTO near-interface region, either during oxide surface preparation or metal evaporation, with dramatic impact on the overall electronic transport.[2,11,13,15] Experiments aimed to better characterize and understand such a complex scenario are crucial for fundamental reasons, and appear of practical relevance for the remarkable role played by metal/NSTO interfaces in several proof-of-concept devices and applications (e.g., ferroelectric RAMs, FETs, photodiodes, resistive switches, spin injecting contacts, and gas sensors).[1,2,16–21] In this respect, methods to determine interfacial conduction and band bending in a spatially resolved way and as a function of the relevant controllable parameters (e.g., doping, stoichiometry, temperature, and environment), offer new opportunities to identify and control the underlying physical mechanisms.[3,22] Hereafter, we use Ballistic Electron Emission Microscopy (BEEM) to investigate prototypical Au/NSTO

Schottky junctions. In BEEM, a Scanning Tunnelling Microscopy (STM) tip at bias V$_T$ injects ballistic electrons into a thin metal overlayer at a constant tunneling current I$_{Tun}$ [Fig. 1(a)]. If the electron energy overcomes the buried energy barrier formed between the metal and the semiconducting substrate, a current I$_{BEEM}$ is transmitted across the sample and collected through the backside Ohmic contact.[23] The Schottky barrier height (SBH) is then defined by the onset of the collector current in I$_{BEEM}$ *vs.* V$_T$ spectra. Our BEEM study gives direct access to the temperature and

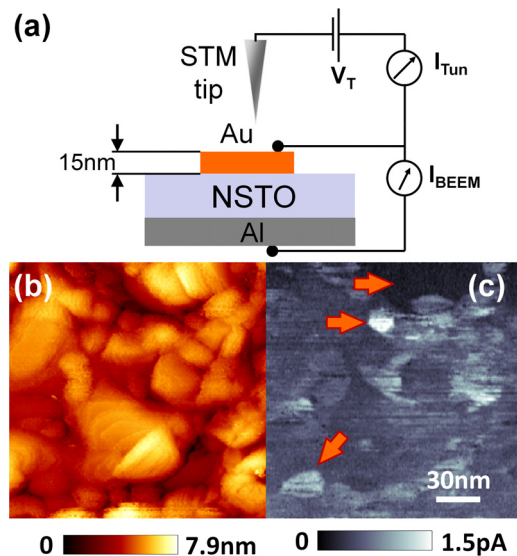FIG. 1. (a) Schematic diagram of the Au/NSTO junction and the experimental setup for BEEM measurements. (b) STM topography and (c) BEEM map acquired simultaneously over a representative Au region (I$_T$ = 45 nA, V$_T$ = −1.85 V, T = 291 K, x_{Nb} = 0.01 wt. %). The arrows highlight a few localized grains with high BEEM contrast.

a)Author to whom correspondence should be addressed: renato.buzio@spin.cnr.it

doping dependence of the SBH, which enables to rationalize puzzling evidences from previous macroscale studies.[7,13,14] Spatially resolved spectroscopy of SBH also allows to quantify the degree of nanoscale interfacial inhomogeneity, that represents a key ingredient to model transport in realistic contacts as well as to address the fundamental relationship between band bending, RS and various sources of interfacial disorder (e.g., defects, impurities or variations in donor concentration).[4,8]

Atomically flat, TiO_2-terminated $SrTiO_3$ surfaces were obtained following the "Arkansas" etching method.[24,25] Briefly, single-crystal substrates of NSTO ($10 \times 5 \times 0.5$ mm^3 by CrysTec GmbH, Germany), with different nominal doping x_{Nb} ($x_{Nb} = 0.01$ wt. %, 0.05 wt. % and 0.5 wt. %), were etched in Aqua Regia (3:1 HCl–HNO$_3$) and annealed for 20 min at 1100 °C in flowing O_2 at a rate of 120 lh^{-1}.[1,8] The Schottky junctions were prepared by depositing 15 nm thick Au electrodes on NSTO by thermal evaporation in vacuum (base pressure $<10^{-7}$ torr, rate $\sim$1.5 nm/min) with a shadow mask (area 2.3 ± 0.1 mm^2). The Ohmic contact was fabricated by depositing aluminium onto the backside of the substrate by pulsed laser deposition. The Au electrode was contacted as reported elsewhere.[1,8,26,27] Macroscopic current-voltage measurements acquired under ultra-high-vacuum (UHV) showed bipolar RS for all diodes,[1,8] with an effective SBH $\phi_{I-V} \approx 1.05$–1.08 eV in the high-resistance state and at room temperature (RT) (see supplementary material S1). Overall, the transport properties were in line with a number of studies for such an interface.[7,8,13] BEEM was performed under UHV using a commercial STM (LT-STM by Omicron Nanotechnology GmbH Germany)[28] equipped with an additional low-noise variable-gain current amplifier (custom DLPCA-200 by FEMTO GmbH Germany).[8,26,27] We used Au tips that were negatively biased ($V_T < 0$), meaning that tunnelling electrons are injected from the tip to the Au electrode. As discussed above, ballistic current I_{BEEM} originates from hot electrons collected at the backside Ohmic contact, after travelling across the sample with kinetic energy e$|V_T|$ high enough to overcome the local energy barrier ϕ_{B0} formed at the buried unbiased Au/NSTO interface [Fig. 1(a)].

Figures 1(b) and 1(c) show typical RT morphology and BEEM maps acquired over a representative region of the Au electrode (qualitatively similar maps were recorded for different temperatures and doping). The topography, which is edge enhanced for visualization purposes, reveals a granular structure with grains $\sim$30–60 nm in diameter. The associated BEEM map appears to some extent correlated with the granular morphology, as the spatial variations of ballistic current I_{BEEM} localize at grains boundaries and very intense contrast ($\sim$50%–100%) occurs at a few specific grains. The current amplitude however does not change systematically with the local surface slope or the thickness of the Au film[8] and BEEM contrast very likely reflects multiple contributions, from the polycrystalline nature of the Au film and from lateral inhomogeneity in the electronic, chemical or spatial structure of the Au/NSTO interface (see below). To gain deeper insight, BEEM spectroscopy was carried out at variable temperature (T = 80 K–295 K). For the acquisition of each BEEM spectrum, the tip voltage V_T was ramped under feedback control, in this way keeping the tunnelling current

($I_{Tun} \sim$30–50 nA) constant. For each nominal doping x_{Nb}, we examined an ensemble of about 3500 spectra, acquired at randomly selected Au surface spots in form of square grids of 150×150 nm^2 area. In Fig. 2(a), we exemplify the BEEM response for $x_{Nb} = 0.01$ wt. %, by comparing two representative raw spectra acquired, respectively, at RT and 80 K on the same Au/NSTO junction. Each spectrum shows a monotonic behaviour, with the characteristic threshold $V_{th,SB}$ corresponding to the local value of the Schottky barrier height, $\phi_{B0} = e|V_{th,SB}|$. Notably, on reducing T from 291 K to 80 K, ϕ_{B0} decreases from $\sim$1.34 eV to $\sim$1.12 eV, whereas the hot electron injection efficiency I_{BEEM}/I_{Tun} grows from $\sim 1 \times 10^{-5}$ up to $\sim 5 \times 10^{-5}$ at $\sim$−1.8V. Figure 2(b) shows that temperature effects are pretty weak for $x_{Nb} = 0.5$ wt. %, since ϕ_{B0} only slightly decreases from $\sim$1.27 eV to $\sim$1.24 eV when reducing T from 295 K to 80 K. The same trends stem out even more clearly for spectra with an improved signal-to-noise ratio, obtained by spatial averaging of neighbor raw spectra over nanometric areas (supplementary material S2). We further explored this phenomenology quantitatively, by fitting individual spectra with the Bell and Kaiser (BK) model $I_{BEEM}/I_{Tun} = R(V_T - V_{th,SB})^2$ (fitting range -0.4 V $< V_T < -1.9$ V) to estimate local values of Schottky
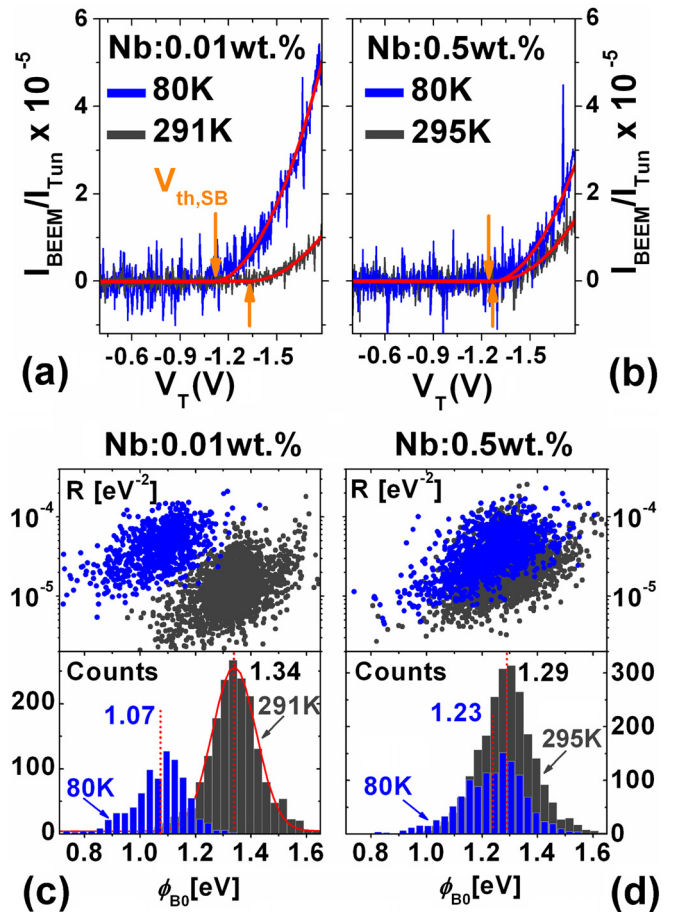
FIG. 2. Representative raw spectra acquired at different temperatures on Au/NSTO junctions with (a) x_{Nb}=0.01 wt. % and (b) x_{Nb}=0.5 wt. %. The red lines are fits with the BK model. (c) Dual parameter (ϕ_{B0}, R) distributions (top) and ϕ_{B0} histograms (bottom) for x_{Nb}=0.01 wt. %, at the two temperatures indicated in (a). Gaussian fits (e.g., the red curve) give the average SBHs at 291 K (1.34 eV) and 80 K (1.07 eV). (d) as in (c) but for x_{Nb}=0.5 wt. %.

barrier height $\phi_{B0} = e|V_{th,SB}|$ and transmission attenuation factor R. The related dual parameter (ϕ_{B0}, R) distributions and the ϕ_{B0} histograms are reported in Figs. 2(c) and 2(d). Local variations in the intensity and onsets of BEEM spectra within each grid caused a remarkable spreading of the ϕ_{B0} and R parameters. This also agrees with the large fluctuations of current intensity observed in the BEEM maps [Fig. 1(c)]. For $x_{Nb} = 0.01$ wt. % [Fig. 2(c)], the barrier spread at 291 K is from $\sim$1.0 eV up to $\sim$1.5 eV, and ballistic transmittance R varies from $\sim 4 \times 10^{-6}$ eV^{-2} up to 1×10^{-4} eV^{-2}. The Gaussian histogram of SBH is centered at the mean (ensemble-averaged) value $\bar{\phi}_{B0} \approx 1.34$ eV, very close to the highest effective barriers reported in literature for the same doping ($\sim$1.4 eV)[7,13] and to predictions from the Schottky-Mott limit ($\sim$1.2–1.3 eV).[1,8,29] The statistical spread of the histogram originates from two distinct contributions, namely the spatial variations of the barrier height at the buried interface and the measurement noise.[30] Careful analysis indicates that experimental uncertainty contributes to the spread with $\sim$50 meV at RT and $\sim$25 meV at 80 K (see supplementary material S2); hence, the actual barrier inhomogeneity at the Au/NSTO can be evaluated to be $\sigma_{0.01\,wt.\%}(291\,K) \sim 85$ meV (standard deviation). At the lower temperature T = 80 K, the distribution (ϕ_{B0}, R) shifts laterally, corresponding to an overall reduction of the local ϕ_{B0} values and a concomitant increase in the ballistic transmittance R. The SBH histogram is centred at $\bar{\phi}_{B0} \approx 1.07$ eV and $\sigma_{0.01\,wt.\%}(80\,K) \sim 100$ meV. For the higher doping case, $x_{Nb} = 0.5$ wt. % [Fig. 2(d)], the statistical spread of ϕ_{B0} and R is comparable with the low doping case, and the SBH histogram at RT is centered at $\bar{\phi}_{B0} \approx 1.29$ eV$[\sigma_{0.5\,wt.\%}(295\,K) \sim 95$ meV]. However, both the (ϕ_{B0}, R) distribution and the ϕ_{B0} histogram are weakly affected by temperature, as the mean SBH decreases with T by only $\sim$0.06 eV $[\sigma_{0.5\,wt.\%}$ (80 K)$\sim$117 meV]. Overall, BEEM indicates that $\bar{\phi}_{B0}$ changes by about 0.3 eV from 80 K to RT for junctions with low (0.01 wt. %) or intermediate (0.05 wt. %) doping (see supplementary material S3), whereas a small variation of $\sim$0.06 eV affects the mean SBH for highly doped (0.5 wt. %) junctions.

Spatially resolved maps of the local barrier height ϕ_{B0} and ballistic transmittance R did not reveal simple correlations with the Au morphology (see supplementary material S4 for maps of ϕ_{B0} and R). On the one hand, the heterogeneity of ϕ_{B0} occurred randomly over most of the interface, with a characteristic length scale of tens of nanometers. On the other hand, large-sized ($\sim$60–90 nm) patches of uniform transmittance R were very common; they typically involved several neighbour grains and showed very good correlation with the spatial features of the related BEEM maps. Thus, we argue that the heterogeneity of the BEEM contrast [depicted in Fig. 1(c)] was mostly the result of inhomogeneity of the local ballistic transmittance R, typically by factors $\sim$2 to $\sim$5. In this respect, the polycrystallinity of Au is by itself sufficient to explain such large fluctuations of R, as grains with various orientations differently affect hot electrons scattering at metal/metal and metal/semiconductor interfaces.[31] Differently, more mechanisms might contribute to the spread σ of the nanoscale SBH. General predictions from "donor-type" deep levels model[32] together with first-principle calculations on Au/Nb:TiO$_2$ junctions[33] and Au/

NSTO indicate that the SBH is greatly sensitive to the concentration and position of oxygen vacancies and Nb dopants within the NSTO near-interface region; hence, sizable fluctuations of SBH are expected. Fluctuations of SBH might also reflect local work-function differences ($\sim$0.05–0.2 eV)[34,35] between the majority TiO$_2$ termination and some minority SrO-terminated regions, as SrO surface segregation can appear under thermal annealing of the NSTO substrates.[15,34] Furthermore, the small yet systematic increase in the barriers spread with doping ($\sigma_{0.5\,wt.\%} > \sigma_{0.01\,wt.\%}$) signals a sizable contribution from the screening properties of the NSTO semiconductor.[36]

We now focus on the temperature dependence of the mean SBH, $\bar{\phi}_{B0}$ (see supplementary material S5 for the T-dependence of $\bar{R}$).

Figure 3(a) shows that in the range from 160 K up to RT, the variation of $\bar{\phi}_{B0}$ is fairly weak regardless of the nominal doping. However, for 80 K $\leq$ T < 160 K, $\bar{\phi}_{B0}$ varies by $\sim$200 meV for $x_{Nb} = 0.01$ wt. %, and by only $\sim$40 meV for $x_{Nb} = 0.5$ wt. %. Note that $\bar{\phi}_{B0}$ results from an ensemble average conducted over a large number of $\phi_{B0}(T)$ values (e.g., $\sim$840 at 80 K and $\sim$1800 at 291 K for x_{Nb} = 0.01 wt. %; $\sim$1200 at 80 K and $\sim$2300 at 295 K for x_{Nb} = 0.5 wt. %); hence, the temperature evolution is robust against experimental noise. The fact that $\bar{\phi}_{B0}$ is largely controlled by doping for T < 160 K deserves special attention, particularly because macroscale studies give apparently contradictory results on this issue due to differences in the interfacial quality, electrostatic analysis and/or transport modelling
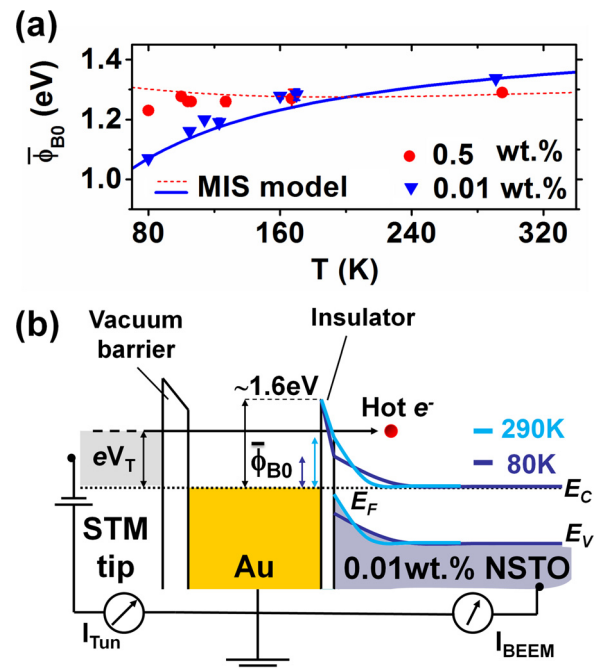

FIG. 3. (a) Temperature dependence of the spatially averaged SBH $\bar{\phi}_{B0}$ measured by BEEM for Au/NSTO junctions with two different doping levels. The solid and dashed lines are theoretical predictions with the metal-insulator-semiconductor (MIS) model. (b) Schematics of the energy band diagram for the *low-doped* unbiased junction (not in scale). Hot electrons emitted by the STM tip with high enough kinetic energy, tunnel across the thin insulator layer[27,37] into the conduction band of NSTO and generate a ballistic current I$_{BEEM}$. The onset of ballistic current, $\bar{\phi}_{B0}$, varies according to the temperature evolution of the NSTO surface potential at the insulator/NSTO interface.

of the Au/NSTO junction. In fact, for a low Nb content of 0.005–0.01 wt. %, Shimizu and Okushi[13] found ∼500 meV increase in ϕ_{I-V} when going from 93 K to 293 K, whereas Hasegawa and Nishino[14] and Susaki *et al.*[7] claimed a temperature-independent SBH in the same T range. In the present case, BEEM probes unbiased junctions; hence, Fig. 3(a) demonstrates that the assumption of a T-independent SBH is acceptable only for sufficiently large temperatures, e.g., T >160 K. Following early studies,[13,38] the T-dependence of interfacial band bending can be ascribed to two concurrent factors, namely the temperature-dependent permittivity of NSTO and the presence of a low-permittivity interfacial layer making the junction to behave as a metal-insulator-semiconductor (MIS) system. According to literature, the interfacial layer likely originates from the interplay of intrinsic contributions, associated with the finite electrostatic screening length in the Au layer,[13,39,40] and extrinsic factors related to unintentional carbon contamination and interfacial defects and/or disorder generated either during the NSTO high-temperature oxidation and the polycrystalline Au growth.[2,15] In this framework, we have found that an MIS electrostatic analysis[11] of the Au/insulator/NSTO heterostructure reasonably agrees with the *low-doped* junctions data of Fig. 3(a) (see supplementary material S6), provided that a constant areal capacitance C_{ins}^{-1} ∼9 m²/F is attributed to the interfacial layer and that the dielectric permittivity of the 0.01 wt. % doped NSTO is treated through the conventional phenomenological equation[7,38]

$$\varepsilon_r(E,T) = b(T)/\sqrt{a(T) + E^2}, \quad (1)$$

where a(T) and b(T) are temperature-dependent material parameters, and E is the electric field. Since Eq. (1) is derived by approximating the Landau-Ginzburg-Devonshire theory, it is appropriate only when the magnitude of E and the parameter a(T) are in the range of $E < 3a(T)^{1/2}$, which is the case for x_{Nb} = 0.01 wt. %.[6] Accordingly, the monotonic dependence of $\bar{\phi}_{B0}$ on T reflects a progressive redistribution of the flat-band voltage (V_{FB} ∼1.6 eV) between the NSTO depletion layer and the interfacial layer, driven by T-induced variations of the depletion width in between ∼387 nm (at 80 K) and ∼203 nm (at 290 K). A schematic of such temperature evolution of band bending is shown in Fig. 3(b) (see also supplementary material for more details). It is remarkable the excellent agreement between the values of C_{ins}^{-1} and V_{FB} we obtained via interpolation of BEEM data and previous estimates, derived from analysis of macroscopic transport measurements.[7,13,29,38,41] The weak temperature dependence of $\bar{\phi}_{B0}$ for *higher* Nb doping deserves a different explanation. In fact, there are evidences that the NSTO permittivity is both strongly depressed (ε_r ∼25–50)[42,43] and almost temperature-independent[6,44] under the high-intensity internal fields (≥25–50 MV/m) of 0.5 wt. % doped junctions, therefore Eq. (1) does not strictly hold.[6] As a further confirmation, we found that predictions from the MIS model using Eq. (1) are inconsistent with the experimental trend depicted in Fig. 3(a). In fact, we argue that comparable interfacial layers characterize all the prepared samples in view of the similar top electrode processing, but the distribution of the flat-band voltage between the NSTO depletion layer and the

interfacial layer is not affected by temperature at high doping, due to the nearly constant permittivity. This possibly results in the weak T-dependence of $\bar{\phi}_{B0}$ for x_{Nb} = 0.5 wt. %.

This study adds insight to the current understanding of metal/NSTO contacts, including all-oxide heterostructures.[17,21] BEEM investigation confirms the MIS model as a valuable platform, where the T-dependence of the SBH arises from the subtle interplay of interfacial quality (interfacial layer capacitance) and NSTO polarizability. The latter is however critically affected by doping, implying that x_{Nb} control across the 0.05–0.5 wt. % range results in a simple and effective means to activate or suppress temperature effects. Recently, using hard X-ray photoemission spectroscopy (HXPES) on highly doped Pt/NSTO junctions, Hirose *et al.*[6] showed that the spatially averaged Schottky barrier profile is unaffected by temperature within ∼0.1 eV instrumental resolution (50 K ≤ T ≤ 300 K). Such finding perfectly agrees with the weak (∼0.06 eV) temperature evolution revealed by BEEM for $\bar{\phi}_{B0}$ with x_{Nb} = 0.5 wt. %. Hence, BEEM complements and refines HXPES, and strengthens the conclusion that Eq. (1) does not properly describe the dielectric properties of SrTiO₃ under high fields but a reconstruction of this phenomenological model is necessary. This issue is highly relevant to simulations, that often rely on Eq. (1) to model transport in highly doped metal/NSTO[2,4,7,20,45–47] albeit the equation overestimates the T-dependence of $\varepsilon_r(E,T)$ below ∼160 K, as pointed out above. The spatial inhomogeneity of the SBH quantified in the present study, provides a key ingredient to properly describe metal/NSTO contacts. Besides offering an explanation for the emergence of RS at such interfaces,[4,8] inhomogeneity is known to reduce the ultimate performance of practical contacts by promoting transport across highly transmitting low-barrier patches.[32] An evaluation of the inhomogeneity role for Au/NSTO is gained at RT *via* a simplified potential fluctuations model, assuming Gaussian variations of the local barrier height[48] and purely thermionic emission across the transparent interfacial layer.[13] According to this model, macroscopic transport is governed by an effective barrier height $\phi_{eff} = \bar{\phi}_{B0} - \sigma^2/2k_BT$, that amounts to $\phi_{eff} \cong$ 1.10–1.20 eV with the parameters of the BEEM histograms in Figs. 2(c) and 2(d). Notably, ϕ_{eff} is close to $\phi_{I-V} \approx$ 1.05–1.08 eV extrapolated from the RT current-voltage measurements in the high-resistance state. The good match suggests that inhomogeneity lowers ϕ_{I-V} by more than ∼200 meV compared to the ultimate values attainable by ideally homogeneous contacts ($\phi_{eff} = \bar{\phi}_{B0} \cong 1.29 - 1.34$ eV). Hence, barrier inhomogeneity impacts the behaviour of the macroscopic metal/NSTO interface as much as the interfacial structure and chemistry issues.[32,49] Further investigations are required to improve our capability to control and predict the response of NSTO-based Schottky contacts. Indeed, besides being highly sensitive to ambient oxygen (see supplementary material S1 and Refs. 1 and 3), the interfacial properties of metal/NSTO greatly vary with fabrication and postprocessing treatments. This makes crucial to assess how inhomogeneity evolves when metallization techniques and deposition protocols drive metal growth towards epitaxy,[2] or when postprocessing (i.e., O₂ postannealing)[50] is applied to reduce interfacial defects and disorder (see supplementary material

S6). From a different perspective, the comprehensive BEEM determination of interfacial potential fluctuations over a length scale of tens of nanometers provides a solid ground to the "regime of random statistical fluctuations,"[51] that was shown to dominate transport in miniaturized Au/NSTO junctions as they are downscaled below the critical size of $\sim$70 nm.

See supplementary material for macroscale current-voltage-temperature characteristics and oxygen sensitivity (S1), BEEM noise contributions (S2), BEEM data for intermediate Nb doping (S3), examples of spatially resolved Schottky barrier and transmittance maps (S4), temperature-dependent ballistic transmittance (S5), and electrostatic MIS model of the junction (S6).

[1]R. Buzio, A. Gerbi, A. Gadaleta, L. Anghinolfi, F. Bisio, E. Bellingeri, A. S. Siri, and D. Marrè, Appl. Phys. Lett. **101**, 243505 (2012).

[2]E. Mikheev, B. D. Hoskins, D. B. Strukov, and S. Stemmer, Nat. Commun. **5**, 3990 (2014).

[3]C. Baeumer, N. Raab, T. Menke, C. Schmitz, R. Rosezin, P. Müller, M. Andrä, V. Feyer, R. Bruchhaus, F. Gunkel, C. M. Schneider, R. Waser, and R. Dittmann, Nanoscale **8**, 13967 (2016).

[4]J. Li, N. Ohashi, H. Okushi, and H. Haneda, Phys. Rev. B **83**, 125317 (2011).

[5]N. Ohashi, H. Yoshikawa, Y. Yamashita, S. Ueda, J. Li, H. Okushi, K. Kobayashi, and H. Haneda, Appl. Phys. Lett. **101**, 251911 (2012).

[6]S. Hirose, H. Okushi, S. Ueda, H. Yoshikawa, Y. Adachi, A. Ando, T. Ohsawa, H. Haneda, and N. Ohashi, Appl. Phys. Lett. **106**, 191602 (2015).

[7]T. Susaki, Y. Kozuka, Y. Tateyama, and H. Y. Hwang, Phys. Rev. B **76**, 155110 (2007).

[8]A. Gerbi, R. Buzio, A. Gadaleta, L. Anghinolfi, M. Caminale, E. Bellingeri, A. S. Siri, and D. Marrè, Adv. Mater. Interfaces **1**, 1300057 (2014).

[9]E. M. Bourim and D. W. Kim, Curr. Appl. Phys. **13**, 505 (2013).

[10]K. G. Rana, V. Khikhlovskyi, and T. Banerjee, Appl. Phys. Lett. **100**, 213502 (2012).

[11]A. M. Kamerbeek, T. Banerjee, and R. J. E. Hueting, J. Appl. Phys. **118**, 225704 (2015).

[12]H. X. Lu, Y. B. Liu, Y. S. Chen, J. Wang, B. G. Shen, and J. R. Sun, J. Appl. Phys. **116**, 173710 (2014).

[13]T. Shimizu and H. Okushi, J. Appl. Phys. **85**, 7244 (1999).

[14]H. Hasegawa and T. Nishino, J. Appl. Phys. **69**, 1501 (1991).

[15]R. Meyer, A. F. Zurhelle, R. A. De Souza, R. Waser, and F. Gunkel, Phys. Rev. B **94**, 115408 (2016).

[16]J. Hou, H. Zhu, J. C. Reed, F. Yi, E. Cubukcu, and D. A. Bonnell, Appl. Phys. Lett. **110**, 43103 (2017).

[17]Z. Xi, J. Ruan, C. Li, C. Zheng, Z. Wen, J. Dai, A. Li, and D. Wu, Nat. Commun. **8**, 15217 (2017).

[18]A. M. Kamerbeek, P. Högl, J. Fabian, and T. Banerjee, Phys. Rev. Lett. **115**, 136601 (2015).

[19]T. Ming, J. Suntivich, K. J. May, K. A. Stoerzinger, D. H. Kim, and Y. Shao-Horn, J. Phys. Chem. C **117**, 15532 (2013).

[20]A. Verma, S. Raghavan, S. Stemmer, and D. Jena, Appl. Phys. Lett. **105**, 113512 (2014).

[21]Y. Bai, Z. J. Wang, J. Z. Cui, and Z. D. Zhang, J. Phys. D: Appl. Phys. **51**, 205303 (2018).

[22]K. G. Rana, S. Parui, and T. Banerjee, Phys. Rev. B **87**, 85116 (2013).

[23]M. Prietsch, Phys. Rep. **253**, 163 (1995).

[24]M. Kareev, S. Prosandeev, J. Liu, C. Gan, A. Kareev, J. W. Freeland, M. Xiao, and J. Chakhalian, Appl. Phys. Lett. **93**, 61909 (2008).

[25]R. C. Hatch, M. Choi, A. B. Posadas, and A. A. Demkov, J. Vac. Sci. Technol. B **33**, 061204 (2015).

[26]R. Buzio, A. Gerbi, D. Marré, M. Barra, and A. Cassinese, J. Vac. Sci. Technol. B **34**, 041212 (2016).

[27]R. Buzio, A. Gerbi, D. Marrè, M. Barra, and A. Cassinese, Org. Electron. **18**, 44 (2015).

[28]A. Gerbi, R. Buzio, S. Kawale, E. Bellingeri, A. Martinelli, C. Bernini, C. Tresca, M. Capone, G. Profeta, and C. Ferdeghini, J. Phys.: Condens. Matter **29**, 485002 (2017).

[29]C. Park, Y. Seo, J. Jung, and D.-W. Kim, J. Appl. Phys. **103**, 54106 (2008).

[30]C. Troadec and K. E. J. Goh, Vac. Sci. Technol. B **28**, C5F1 (2010).

[31]P. Niedermann, J. Vac. Sci. Technol., B: Microelectron. Nanometer Struct. -Process., Meas., Phenom. **10**, 580 (1992).

[32]R. T. Tung, Appl. Phys. Rev. **1**, 011304 (2014).

[33]Y. Jiao, A. Hellman, Y. Fang, S. Gao, and M. Käll, Sci. Rep. **5**, 11374 (2015).

[34]L. Aballe, S. Matencio, M. Foerster, E. Barrena, F. Sánchez, J. Fontcuberta, and C. Ocal, Chem. Mater. **27**, 6198 (2015).

[35]M. Mrovec, J.-M. Albina, B. Meyer, and C. Elsässer, Phys. Rev. B **79**, 245121 (2009).

[36]H. Palm, M. Arbes, and M. Schulz, Phys. Rev. Lett. **71**, 2224 (1993).

[37]K. E. J. Goh, A. Bannani, and C. Troadec, Nanotechnology **19**, 445718 (2008).

[38]S. Suzuki, T. Yamamoto, H. Suzuki, K. Kawaguchi, K. Takahashi, and Y. Yoshisato, J. Appl. Phys. **81**, 6830 (1997).

[39]Y. Hikita, M. Kawamura, C. Bell, and H. Y. Hwang, Appl. Phys. Lett. **98**, 192103 (2011).

[40]M. Stengel and N. A. Spaldin, Nature **443**, 679 (2006).

[41]Y. Hikita, Y. Kozuka, T. Susaki, H. Takagi, and H. Y. Hwang, Appl. Phys. Lett. **90**, 143507 (2007).

[42]T. Fujii, M. Kawasaki, A. Sawa, Y. Kawazoe, H. Akoh, and Y. Tokura, Phys. Rev. B: Condens. Matter Mater. Phys. **75**, 165101 (2007).

[43]A. Ruotolo, C. Y. Lam, W. F. Cheng, K. H. Wong, and C. W. Leung, Phys. Rev. B **76**, 75122 (2007).

[44]R. A. van der Berg, P. W. M. Blom, J. F. M. Cillessen, and R. M. Wolf, Appl. Phys. Lett. **66**, 697 (1995).

[45]P. Han, J. F. Jia, and M. He, Appl. Surf. Sci. **255**, 6262 (2009).

[46]M. Yang, X. Ma, H. Wang, L. Xi, L. Lv, P. Zhang, Y. Xie, H. Gao, Y. Cao, S. Li, and Y. Hao, Mater. Res. Express **3**, 75903 (2016).

[47]T. Chien, J. Liu, A. J. Yost, J. Chakhalian, J. W. Freeland, and N. P. Guisinger, Sci. Rep. **6**, 19017 (2016).

[48]J. H. Werner and H. H. Güttler, J. Appl. Phys. **69**, 1522 (1991).

[49]T. Tachikawa, H. Y. Hwang, and Y. Hikita, Appl. Phys. Lett. **111**, 91602 (2017).

[50]D. S. Shang, J. R. Sun, L. Shi, J. Wang, Z. H. Wang, and B. G. Shen, Appl. Phys. Lett. **94**, 052105 (2009).

[51]J. Hou, S. S. Nonnenmann, W. Qin, and D. A. Bonnell, Appl. Phys. Lett. **103**, 252106 (2013).